J. Phys. D: Appl. Phys. **42** (2009) 155201 (8pp) doi:10.1088/0022-3727/42/15/155201

Ion acceleration at different stages of a pulsed vacuum arc

V L Paperny[1], A A Chernich[1], N V Astrakchantsev[2] and N V Lebedev[2]

[1] Department of Physics, Irkutsk State University, Irkutsk 664003, Russia
[2] Institute for Physics and Technology, Irkutsk State Technical University, Irkutsk 664040, Russia

Received 4 February 2009, in final form 27 April 2009
Published 7 July 2009
Online at stacks.iop.org/JPhysD/42/155201

Abstract
Detailed measurements of ion energy distributions (IEDs) originating at different stages of a pulsed vacuum arc are studied. It is shown that for a variety of cathode materials (Al, Mg, Ti and Zr), the directed energies per charge unit of ion originating at the initial stage of the arc, i.e. in 25 μs after ignition, are close to each other and are, approximately, as much as $E_{\mathrm{dir}}/Z \approx 70$ eV. A non-Maxwellian shape of these IEDs that is due to the presence of significant 'tails' of ions accelerated up to energies of a few hundred eletronvolts is found. In 100 μs after the arc ignition the directed energies relax to values that are close, principally, to values that have been measured earlier elsewhere. It is found that the 'anomalously' accelerated ions propagate within a narrow angle that is as much as, approximately, $\pm 15^{\circ}$ in relation to the plasma flux axis. These characteristics suggest that beyond the commonly adopted gas-dynamic mechanism of ion acceleration in cathode micro-jets, at the initial stage of a pulsed arc the mechanism of additional ion acceleration is presented, which is due, obviously, to a self-consistent electric field arising in front of the plasma macro-jet.

1. Introduction

It is well known that vacuum discharge plasma is produced at non-stationary cathode jets of micrometre size ejected from a cathode surface, which are characterized by extremely high current density, power density and plasma density. Due to these parameters in these micro-jets, ions of the cathode material at high charge states are produced and acceleration of these ions up to high velocities occurs. Directed ion energies for most of the materials are in the range from 20 to 150 eV [1]. The majority of ion energy studies deal with the average or the most likely ion energy, which was obtained by different modifications of the time-of-flight method [2–5]. These studies demonstrate that energies of different ion species are approximately independent of the ion charge states [5, 6]. More precise measurements of ion energy distributions (IEDs) for specified ion charge states by electrostatic analyzers exhibit a rather discrepant picture. Measurements of Anders and Oks [7], Galonska *et al* [8] and Chhowalla [9] supported the results mentioned above; thereafter Kutzner and Miller [10] and Lunev *et al* [11] revealed an increase in ion energy with charge state for a number of cathode materials. Recently, Rosén *et al* [12] found the same effect with an aluminium plasma.

The other 'mysterious' effect found at the pulsed vacuum arcs was relatively enhanced values of both ion charge states and velocities, which were observed at the beginning of the pulse. These parameters decreased throughout the pulse down to steady-state average values, which were approached in a few hundred microseconds after the discharge ignition (see, for instance, [1, 13–15]). The detailed measurements of IED with different durations of a pulsed discharge also revealed that both the most likely energies and widths of the distributions were enhanced at a short pulse duration as compared with the longer one [7]. Note that in [7] the IED *averaged* over the pulse length has been measured.

Several theories have been suggested to account for the ion acceleration mechanisms leading to the energies observed. The two most referred to are the potential hump theory [16] and the gas-dynamic model [17, 18]. The former predicts ion formation near the peak of the discharge voltage profile and acceleration due to the electric field, and the latter states that the ion acceleration occurs within plasma cathode micro-jets of a micrometre scale, and the electron–ion friction and pressure gradient are the main mechanisms responsible. The gas-dynamic model was supported by the extended studies using a number of elements (about 50) as cathode materials in a pulsed vacuum arc [1]. Notice that these results were

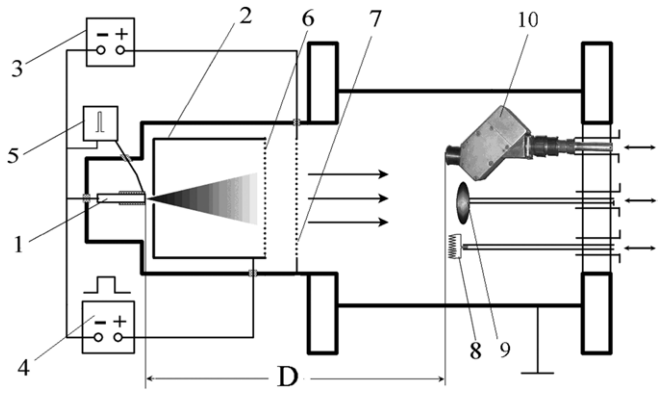

Figure 1. Experimental setup (MEVVA. RU) 1, cathode; 2, anode; 3, accelerating voltage supply (was not in use); 4, discharge supply; 5, trigger pulse supply; 6, anode grid; 7, accelerating grid; 8, heated probe; 9, Langmuir probe; 10, ion energy analyzer.

obtained for the steady-state stage of a pulsed discharge, about 150 μs after the discharge ignition. So we suggest that it is the gas-dynamic model that adequately explains the principal features of ion production and acceleration in cathode micro-jets. Nevertheless, at the moment, the model cannot explain the enhanced ion velocities that were observed at the beginning of a pulsed arc and the increase in ion directed energy with ion charge state that was observed in a few experiments. Hence, additional studies are needed to clarify the problem of ion acceleration in pulsed vacuum discharges.

This paper presents a fresh approach to the study of the temporal change of parameters of ion component in pulsed arc, namely, the use of an advanced diagnostic allows us to perform detailed studies of changes in the IED throughout a pulsed vacuum arc for a set of cathode materials with different physical characteristics. The objective of the studies is to establish distinctive features of the 'anomalous' ion acceleration at the initial stage of a pulsed arc.

2. Experimental setup and measurement procedure

The experiments were performed with a pulsed vacuum arc of the MEVVA type [5] that is depicted in figure 1. The electrode array comprised a cylindrical cathode of 6 mm diameter (1) and an annular anode with an inner diameter of 13 mm (2); the anode was 9 mm away from the cathode surface. The vacuum chamber was evacuated to a residual pressure of 4–6 $\times$ 10^{-6} Torr. The discharge was initiated on the cathode surface by means of a high-voltage breakdown via a dielectric insert between the cathode and the igniter. The discharge was fed by a LC-pulse line resulting in a current pulse of 150 A amplitude, of 30 μs rise time and of 200 μs duration; the current was measured with the Rogovski coil. The plasma flux leaving the arc discharge region passed through the anode hole and expanded while streaming towards the anode grid (6). Then it passed through the anode grid, the additional accelerating grid (7), which was not used in these studies, and expanded into the equipotential drift chamber with a diameter of 20 cm and a length of 30 cm. Ion current density was measured using a movable flat Langmuir probe (9) operating with a saturation regime and the plasma potential was measured by a movable heated probe (8). It is well known that ion and electron saturation currents at the Langmuir probe sited in a plasma flux moving with a super-sound directed velocity V_i are specified with the relations

$$I_i = A_i S_p n_i Z e V_i \quad \text{and} \quad I_e = A_e S_p n_e e\sqrt{2kT_e/\pi m}, \qquad (1)$$

respectively [19]. Here A_i, A_e are the factors determined by the probe shape and bias; S_p is the effective collecting surface of the probe; n_i and n_e are ion and electron densities, respectively; Z is the mean ion charge state; T_e and m are the electron temperature and mass.

IED of the cathode plasma jet was measured by an electrostatic ion energy analyzer (10) of the 'plane capacitor' type that was placed at a distance $D = 45$ cm from the cathode and was supplied with a microchannel plate as the detector. The analyzer was rotatable within a range of angles with reference to the plasma stream axis. The entrance orifice tube of the analyzer had an aperture of about of 5° and it was grounded. Energy of the recorded ions was specified by the formula $E/Z = \sigma e U_d$. Here U_d is the (positive) voltage applied at the deflecting plate of the analyzer electrodes with reference to the grounded opposite plate and $\sigma \approx 1.4$ is the geometrical factor, which was determined by the design and dimensions of the electrode array. The energy resolution of the energy analyzer was $\Delta E/E = 0.1$. Preliminary experiments showed that the peak of the arc current was less than 150 A and held nearly constant for different cathode materials. Also, the discharge voltage was practically constant for the central part of the arc pulse, i.e. from 20 to 180 μs after ignition.

Figure 3 presents typical waveforms of both the discharge current with a Zr cathode and the analyzer signal at the specified ion energies. With the given voltage applied at the deflecting plate U_d, the analyzer recorded throughout the discharge pulse the ions of *all* charge states Z with the given energy per a charge unit $E/Z = \sigma e U_d$, which move within the aperture of the entrance orifice tube. One can see that the shape of the signal changes significantly with change in the energy recorded. At low energies, the signal is of a bell-like shape with the maximum located close to the termination of the discharge pulse (see figure 3(b)). Note that there are no ions with low energies at the beginning of the pulse. At this stage of the discharge, only ions with higher energies appear (see figure 3(c)) and later, as the energy increases, the maximum of the ion signal becomes more pronounced (figure 3(d) and (e)). As a result, the ions with highest energies are recorded, practically, just at the first 50 μs after the discharge ignition; hence they originated at the front of the discharge pulse (figure 3(f)).

To establish the variation in the parameters of the ion component throughout the discharge pulse, we built up the IED for two groups of ions, which were originated at different instants of the discharge pulse denoted with arrows in figure 3(a). The first instant t_1 corresponds to the initial transient stage of the pulse, approximately 25 μs after ignition, when the discharge current attains a maximum, and the second instant t_2, 100 μs later, denotes the stage when the parameters of the plasma relax to the steady-state values. For each ion

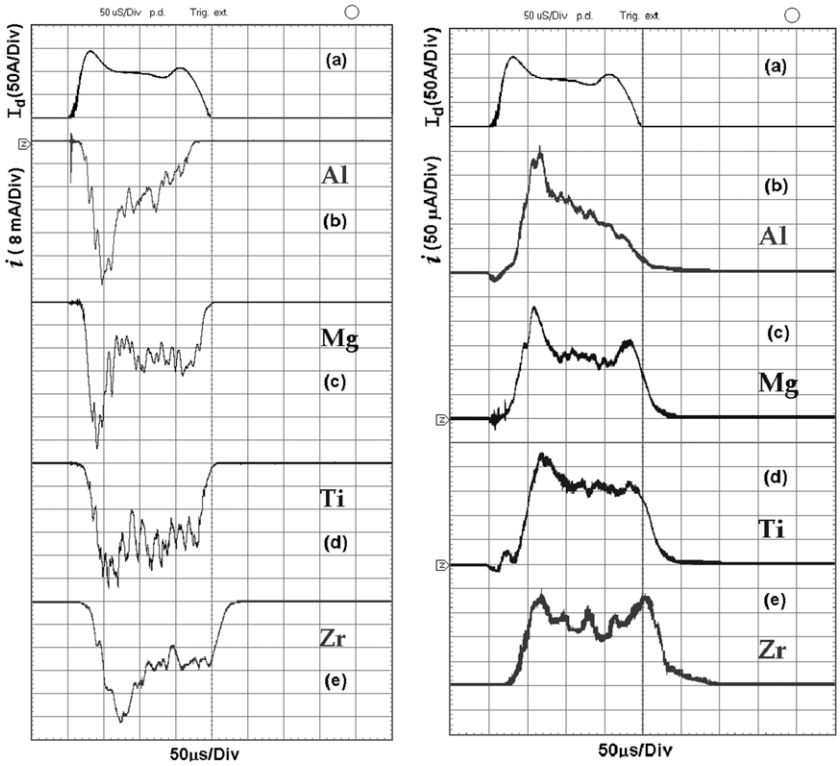

Figure 2. Waveforms of the arc current (a) and Langmuir probe signals (b)–(e) for different cathode materials: electron saturation current (left column) and ion saturation current (right column).

group we calculated the instant of approaching the detector for the specified ion energy E/Z and the given length of ion flight trajectory (it was approximately equal to D in figure 1). These instants are denoted by the corresponding arrows in figure 3(b)–(f)) and just the signals at these instants were used for building up the corresponding IEDs. Each individual measurement was characterized by large shot-to-shot variations of the signals, which is due to the stochastic nature of the plasma jet origin in vacuum arcs and it is quite common for the cathodic arc plasmas, as had been noted earlier, for instance in [20]. Hence, to obtain the statistically justified results, we averaged the analyzer signals over 10 shots with the parameters of the discharge held constant. This procedure was repeated throughout the range of relevant energies and in this way the 'momentary' IEDs for the two ion groups produced at the noted points in time were obtained over a series of 100–200 shots. By this method we recorded ions of all charge states that are present at the plasma jet. In agreement with the results mentioned in section 1, we suggested that all ion species for the given cathode material had energies lying close to each other; hence, in fact, we built up the distribution of ions over energy per mean ion charge unit $E/\bar{Z}$, where the mean ion charge state $\bar{Z}$ was the characteristic for the given material of the cathode.

3. Results and discussion

First, let us consider the results of the probe measurements. In figure 2 the typical waveforms of both ion and electron saturation currents at the probe for a variety of cathode materials in use are presented. One can observe that there are bursts at the beginning of the discharge pulse, which are clearly pronounced for materials with low melting points, i.e. for Al and Mg, and are seen rather less for refractive metals, namely, for Ti and Zr. Also note that the bursts are present at both the ion and the electron signals. As relations (1) show, the ion saturation current is governed by both the density and the velocity of ions of the plasma flux, while the electron saturation current is governed by the electron density and the temperature. The additional measurements found that the electron temperature is held nearly constant throughout the pulse, hence, the following conclusion may be drawn from the probe data: it is an enhancement of the plasma density at the beginning of the discharge that is, principally, responsible for the bursts observed at the probe signals.

Now let us consider the results of the ion analyzer measurements. The 'momentary' IEDs for both the ion groups, which are measured with the entrance orifice of the analyzer oriented along the plasma jet axis, are presented in figure 4. One can see that the peak of the IED (corresponding to the most likely energy) for the first ion group lies near 70 eV and it is near 40 eV for the second one. Furthermore, the former exhibits a pronounced 'tail' of ions with energies up to a few hundred electronvolts, so that the average energy of these ions is rather higher than that of the second ion group. Both the maximum and the area occupied by the IED of the first ion group significantly exceed those of the second group, hence the yield of the first ion group significantly exceeds that of the second one as well. From figures 3 and 4 one can conclude that (i) ions with low energies are produced, principally, after the

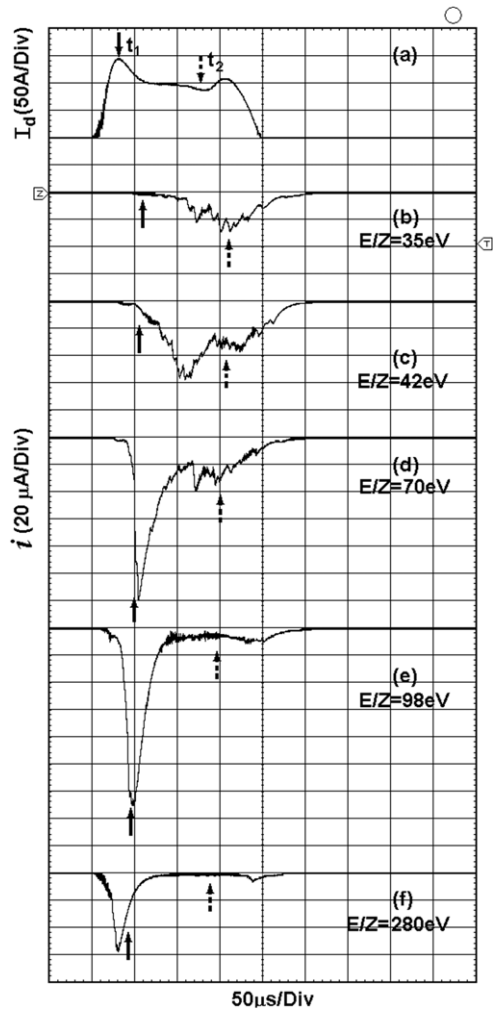

Figure 3. Waveforms of discharge current for Zr cathode (a) and ion analyzer signal at the specified recorded energies (b)–(f). Solid arrow in curve (a) denotes the instant of origination of the first ion group and dashed arrow denotes the instant of origination of the second ion group, corresponding arrows in panels (b)–(f) denote the instants when these ion groups approach the analyzer.

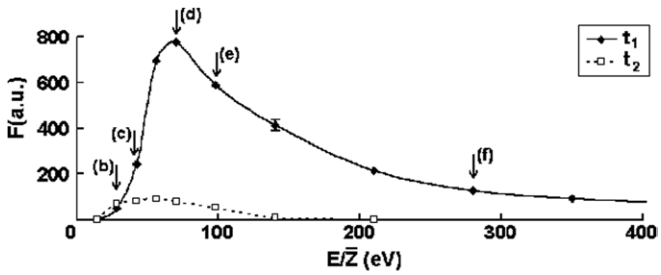

Figure 4. IEDs of two ion groups built up from data of figure 3. Arrows point out the energies that are presented in figure 3.

peak of the discharge current is attained, i.e. at the steady-state stage of the discharge; (ii) ions from the peak of the current correspond to the peak of the analyzer signal, i.e. they have, dominantly, the most likely energy of the IED; (iii) ions with high energies from the 'tail' of IED originated at the front of the current pulse.

Figure 5 presents the IEDs for different cathode materials. One can see from figure 5(*a*) that the IEDs for the first ion group

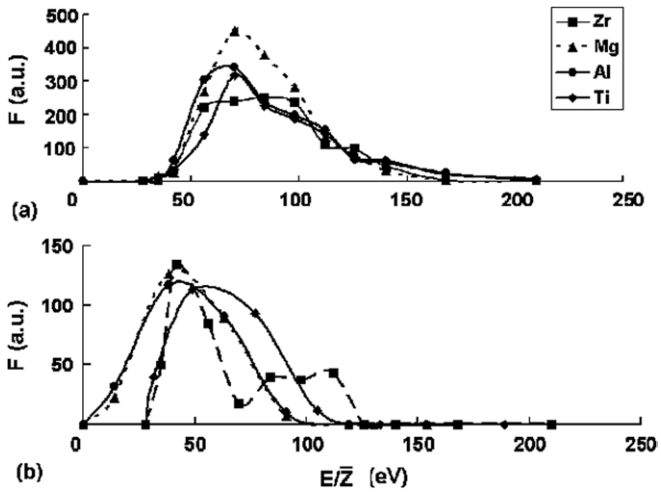

Figure 5. IEDs built up for a variety of materials of cathode for the first ion group (*a*) and for the second one (*b*).

for all the materials under consideration are of similar shape and the most likely energies lie close to each other. Also, it should be noted that all the distributions have the 'tails' of the accelerated ions mentioned above. Figure 5(*b*) shows that the most likely energies of the second ion group for all cathode materials are close to 45 eV, but differ slightly for different cathodes. One can see from figure 5(*b*) that these IEDs have rather less width and are of a near bell-like shape as well.

To gain additional information on the plasma parameters, the distributions were fitted by the shifted Maxwellian distributions (SMDs), as done, for instance, by Rosén *et al* [12]. The ion flux distribution of a SMD can be written as

$$f_{\mathrm{SMD}}(E) = C[E - \bar{Z}e\varphi_{\mathrm{pl}}] \times \exp\left[-\left(\frac{\left(\sqrt{E - \bar{Z}e\varphi_{\mathrm{pl}}} - \sqrt{E_{\mathrm{dir}}}\right)^2}{\Delta E}\right)\right],$$

where C is a scaling constant, φ_{pl} is the plasma potential with respect to the reference voltage of the analyzer (ground), E_{dir} is the directed energy of ions and ΔE is the scatter of ion energy, which is due to the stochastic nature of plasma production in cathode micro-jets. The terms containing $\bar{Z}$ are introduced to account for the increase in ion energy due to the difference between the plasma potential φ_{pl} and the analyzer entrance. As mentioned above, the mean ion charge states at the beginning of a pulsed discharge exceed the ones at the steady-state stage, hence we used the corresponding values for both ion groups from [15]. The emission probe measurements show that the plasma potential at the beginning of the pulse is a few eV higher than the one at the steady-state stage, and we used these distinct values at the fittings as well.

Figure 6 shows that the IED of the second ion group can be fitted by a SMD with sufficient accuracy, while the IED of the first ion group cannot be fitted by the SMD with any accuracy because of the presence of the 'tail' of high energy ions. The fitting parameters of the SMD employed for all cathode materials and for both the first (t_1) and the second (t_2) ion groups are presented in table 1. The data show that both

the directed ion energies and the widths of the IEDs of the first ion group significantly exceed those of the second one for all cathode materials. This result is consistent, qualitatively, with the data gained earlier at the MEVVA device with an Al cathode [7].

For comparison, the directed ion energies for the same materials obtained earlier by other authors with steady-state arcs [10, 11] or with pulsed arcs [1, 7, 12] are also shown in table 1. In the pulsed arcs these energies have been measured by the time-of-flight method at the steady-state stage of a pulse, namely, 100–200 μs after arc ignition. Hence, these energies correspond to the second ion group in our experiments. One can see good agreement of the directed energies for refractive metals (Zr and Ti), satisfactory agreement for a metal with a low melting point (Mg) and a significant difference for the other similar metal (Al).

An important characteristic of an ion acceleration mechanism is the dependence of the IED on the angle of ion propagation relative to the plasma flux axis. Earlier, by means of a rotatable cathode assembly [1] or by a movable ion collector [11], the angular dependence of ion flux as well as the averaged ion kinetic energy have been measured, and then the ion flux was averaged over the duration of the pulsed arcs. The diagnostic techniques mentioned above had a wide aperture so they recorded ions moving within a solid angle, approximately, as much as 2π. As distinct from these techniques, our rotatable energy analyzer recorded ions moving just within a narrow angle corresponding to the aperture of the entrance orifice tube of the analyzer, i.e. about 5°. Hence, it allows us to establish the angular dependences of IED with high resolution and for different stages of the discharge.

Figure 7(a) shows that IEDs of the first group of ions are changed significantly with the angle, namely, the extended tail of high energy ions is recorded for ions propagating at a modest angle to the axis of the plasma flow; therewith the tail is absent for ions moving at a marked angle to the axis. The effect results in an abrupt drop in both the average energy and the total number of ions (the latter corresponds to the area occupied by the IED) with increasing angle. The same dependences for the second ion group are rather less pronounced (figure 7(b)). Figure 8 shows that the angular dependences of these parameters for the first ion group, in fact, are rather strongly pronounced as compared with the second one, so that the former lie, principally, within the range of ±15° relative to the axis of the plasma flux.

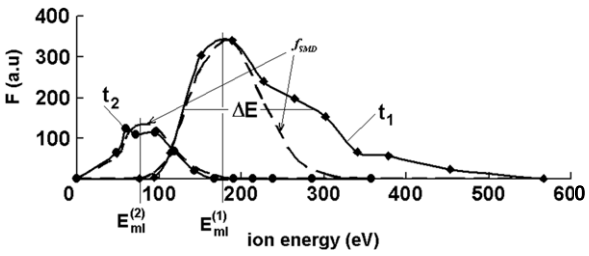

Figure 6. IEDs for two ion groups, fitted with the corresponding SMDs.

Let us sum up and discuss now the distinction between the characteristics of the ion flux at the beginning and at the steady-state stage of the pulsed discharge. Note once more that the directed energies E_{dir} of the former exceed more than two times those of the latter (see table 1), therewith it will be remembered that the measured ion energies at the steady-state stage are close to those which have been measured earlier for a wide set of cathode materials and to those obtained from the gas-dynamic model as well [1]. There may be a variety of sources for this effect. As the first one we suggest that beyond the commonly adopted gas-dynamic ion acceleration in cathode micro-jets, an additional mechanism of acceleration runs at the beginning of a pulsed arc and this mechanism is 'switched off' at subsequent stages of the pulse. This mechanism may occur within a micro-jet that is produced as a result of merging separated micro-jets that occurs at a distance of the order of a millimetre from the cathode surface [21, 23] and it is due to variation throughout a pulse of area of the surface $S_0(t)$ occupied by the cathode spots. We examine this effect in more detail because it has been applied earlier also for explaining the enhancement of the ion charge state at the beginning of a pulsed arc [26].

First, note that it is the area $S_0(t)$ that is reasonable to set equal to the near-cathode root of a plasma flux, which, in turn, governs the plasma density in the near-cathode portion of the flux. As is known [21, 22], spots of widely varying sizes were observed on the cathode surface. It is commonly adopted that a macro-spot with an area in the range $S_0 \approx 10^{-4}$–10^{-3} cm^2 allows a discharge current in the range of 20–200 A to pass through itself [21]; hence in our experiments this macro-spot serves as the root of the cathode plasma macro-jet or integral cathode flux. It is also known that the macro-spot is composed of a number of micro-spots of micrometre size, which are adopted as roots of the micro-jet, where the primary ion production and acceleration due to the gas-dynamic mechanism occur [1, 17, 18].

Now we suggest that at the initial stage of the discharge, approximately $\leqslant 25\,\mu$s after ignition, when the discharge

Table 1. Parameters of ion flux in cathode plasma jet obtained by a variety of research groups.

			Presented results					
			t_1			t_2		
Cathode	Kutzner and Miller [10]	Anders and Yushkov [1]	ΔE	E_{dir}	$\bar{Z}e\varphi_{\mathrm{pl}}$	ΔE	E_{dir}	$\bar{Z}e\varphi_{\mathrm{pl}}$
Al	35	33 (42 [12])	20	160	18	20	70	12
Ti	55	60 (75 [11])	20	165	22	15	75	17
Mg	—	50 (40 [7])	20	130	14	12	60	10
Zr	40	110	20	250	27	10	100	19

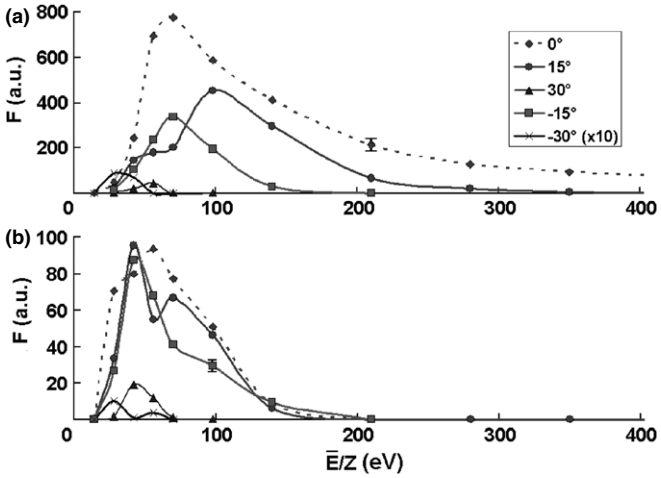

Figure 7. IEDs at different angles of ion propagation relating to the plasma flux axis for the first ion group (*a*) and for the second one (*b*) for Zr cathode.

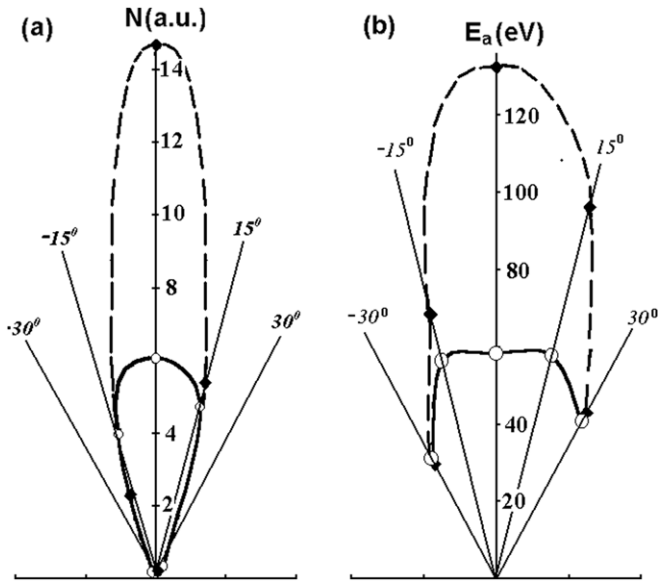

Figure 8. Dependences on the angle of propagation relative to the plasma flux axis of the total number of ions (*a*) and the average ion energy (*b*) for the first ion group (dashed lines) and for the second one (solid lines) for Zr cathode.

current rises rapidly, this macro-spot is located close to the igniter. In the last stage of the discharge, the cathode surface occupied by the micro-spots is enhanced due to their random motion [25]. The characteristic time of the spots spreading over the cathode surface is $\tau_S \approx S/D$, where S is the area of the surface occupied by the spots in time τ_S and $D \approx 5$–$20\,\mathrm{cm^2\,s^{-1}}$ is the diffusion coefficient for the random micro-spots motion [21, 22, 24]. The time for enhancement of the initial area S_0 of the macro-spot lies in the range of $\tau_S \approx 50$–$200\,\mu\mathrm{s}$. Hence, in this time, plasma density in the near-cathode root of a plasma flux $N_e \propto 1/S$ drops an order of value as well. This effect leads to a decrease in the plasma density throughout the plasma flux that is in qualitative agreement with the experimental results presented above.

To demonstrate that a small area of the root of a cathode macro-jet leads to an increase in the directed ion velocity at the initial stage of the discharge, let us consider the results of computer simulations of a cathode plasma flux expansion into the ambient vacuum. We consider a theoretical model that was elaborated earlier by Krinberg and described in detail elsewhere [26, 27], so that we consider here its principal concepts just briefly.

As is known, the motion of a current-carrying plasma is described by the following set of magneto-hydrodynamic equations:

$$\frac{\partial \rho}{\partial t} = -\nabla \cdot (\rho \boldsymbol{V}), \tag{2}$$

$$\rho\left(\frac{\partial \boldsymbol{V}}{\partial t} + \boldsymbol{V}\cdot\nabla\boldsymbol{V}\right) = -\nabla P + \boldsymbol{j}\times\boldsymbol{B}, \tag{3}$$

$$\nabla \times \boldsymbol{B} = \mu_0 \boldsymbol{j}, \tag{4}$$

where $\rho = mN_+$ and $P = kT_eN_e + kT_+N_+$ are the plasma density and pressure, $\boldsymbol{V}$, T_+ and N_+ are the velocity, temperature and number density of ions, $\boldsymbol{j}$ is the current density, $\boldsymbol{B}$ is the magnetic field and μ_0 is the magnetic permeability of free space.

The electron heat balance equation, where electron conductivity and electron energy losses in electron–ion collisions are ignored as compared with the Joule heating and the electron cooling due to the plasma expansion, can be written as

$$\frac{3}{2}P_e\frac{\mathrm{d}_e}{\mathrm{d}t}\ln\left(\frac{P_e}{N_e^{5/3}}\right) = \frac{j^2}{\sigma}, \tag{5}$$

where $\mathrm{d}_e/\mathrm{d}t = \partial/\partial t + V_e\partial/\partial r$ holds, $P_e = kT_eN_e$ and V_e are the electron pressure and velocity and σ is the electrical conductivity.

As a basis for our calculation of the plasma parameters along the interelectrode gap axis, we used the model that employs the following assumptions:

(i) A one-dimensional calculation, which takes into account changes in the plasma flow cross-section, is used.
(ii) The transverse velocity, with which the plasma flux is expanded from its axis, is assumed to be much lower than the velocity with which the plasma propagates towards the anode.
(iii) The plasma parameters T_e, V and $j = I/S$ are taken to be uniform over the flow cross-section.
(iv) The ion pressure is neglected in comparison with the electron pressure in view of the inequality $ZT_e \gg T_+$, characteristic of a cathode plasma. Thus the plasma pressure $P \approx P_e$ holds constant.

To simplify the computation procedure and taking into account the relatively low electron temperature at the given experimental conditions, we consider the ionic composition as being unchanged during plasma flux expansion.

To study the variation in the plasma parameters along the plasma flow, the non-stationary equations (2), (3) and (5) were solved numerically until a steady state was reached under the constant boundary conditions $N_e = N_0$, $T_e = T_0$, $V = V_0$. We used, as input data, the value of arc current I, the root cross-section of the plasma flux S_0 and the plasma

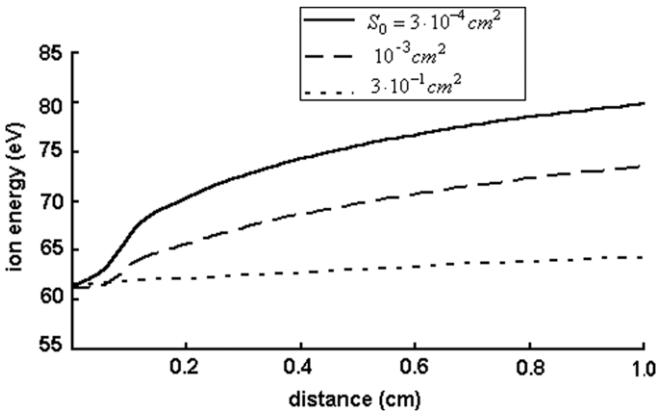

Figure 9. Distribution along the plasma flux of the directed ion energy obtained from the computer simulation for a variety of initial root cross-sections of cathode macro-jet.

parameters of a near-cathode region, which can be taken from measurements. The boundary values can be estimated as follows. It is possible to use, as the ion velocity gained as a result of the primary gas-dynamic acceleration within the cathode micro-jets, $V_0 \approx 1.5 \times 10^4\,\mathrm{m\,s^{-1}}$ for Ti [1] and to obtain the initial electron density from the relations implying that mass and charge fluxes are constant along the plasma flow as follows: $N_0 = \eta_0 I/(eV_0S_0)$, where $\eta_0 \approx 0.09$ is the erosion coefficient for Ti [28]. The boundary electron temperature at the micro-jets merging region is poorly specified and we took as a characteristic value $kT_0 = 1\,\mathrm{eV}$; therewith testing calculations showed a weak dependence of results on the value.

To simulate the initial stage of the fast rise of the discharge current, we solved the non-steady-state equations (2), (3) and (5) numerically by the particle-in-cell method with parameters of the current that are close to those observed in the experiment, namely, the initial rise of the discharge current was taken as

$$I(t) = I_0 + I_a(t/\tau).$$

Here I_a is the peak discharge current, τ is the characteristic time of the current rise and I_0 is the initial current that accounts for the presence of a low-density pre-plasma that is produced by the ignition current and closes the discharge current as the cathode flux propagates towards the anode. Note that testing calculations showed a weak dependence of results on the latter.

Results of the calculation of the IED along the discharge axis for a variety of initial root cross-sections of the cathode macro-jet are presented in figure 9. The figure shows that for a minimum cross-section lying within the range mentioned above, the energy of the plasma jet increases with the distance from the cathode, approximately by a factor of 1.4, which is in satisfactory agreement with the data observed. As the initial cross-section is extended, the energy increase is less pronounced, so that when the cross-section is close to the whole cathode area, the energy increase is negligible. Thus, the simulation demonstrates that, really, the small root cross-section of a cathode macro-jet at the beginning of a pulsed vacuum arc results in a marked additional enhancement of energy of ions, which they gained in the process of primary gas-dynamic acceleration in the micro-jets. The subsequent enhancement of the root cross-section of a cathode macro-jet due to spreading of the micro-spots over the cathode surface results in the 'switching off' of the mechanism of additional ion acceleration. It should be noted that the model presented does not account for the enhancement of the observed ion charge state at the beginning of a pulsed vacuum [15], which would result in a more marked increase in ion energy in the experiment as compared with the simulation.

The mechanism considered above may not be the single cause of the enhanced ion velocity at the beginning of a pulsed vacuum arc. This may also take place immediately within the cathode micro-jets in the course of the primary gas-dynamic ion acceleration and be due to an effect considered by Beilis, who had shown that the velocity that ions gain at the cathode micro-jets, depends substantially on the cathode erosion rate [29]. For instance, decreasing this parameter just from 100 to 70 $\mu\mathrm{G\,C^{-1}}$ at a discharge current of 100 A, results in an increase in the velocity of the Cu ion from 2×10^4 to $4 \times 10^4\,\mathrm{m\,s^{-1}}$. Therewith, it is well known that the erosion rate is a time-dependent parameter, so that at the initial spark stage of a vacuum discharge it is a few times less than the one at the subsequent arc stage [30]. Hence, if one suggests that there is a relatively low cathode erosion rate at the initial transient stage of the discharge then the enhanced ion velocities should be attained here. The subsequent transition of the discharge to a quasi-steady arc stage results in enhancement of the erosion rate which, in turn, leads to the relaxation of the ion velocity to the 'standard' value observed both in the present measurements and in those performed earlier.

It should be emphasized that both mechanisms of the 'anomalous' ion acceleration at the beginning of a pulsed arc considered above are of a hydrodynamic origin, hence they result in equilibrium, i.e. the Maxwellian shape of the IED. Nevertheless, a distinguishing feature of the distribution at the given experiments is the presence of extended 'tails' of fast ions with energies of a few hundred electronvolts. Also, recall that the most likely energies per charge unit E_{ml}/Z for ions of different cathode materials lie close to each other, as shown in figure 5(*a*). Even if we take into account the plasma potentials, which differ for these materials, this statement remains valid in principle. These distinguishing features of the IED at the beginning of the pulse allow us to assume that the additional ion acceleration, obviously, is governed rather by an electric field that arises at the beginning of the pulse than the hydrodynamic mechanisms considered above. In this case, the commonly adopted primary gas-dynamic ion acceleration is valid, virtually, in the cathode micro-jets.

The reasons for the production of the suggested self-consistent electrical field are not yet clear. A possible reason is ejection of a flow of accelerated electrons from a plasma jet with a pulsed arc that has been revealed in [31]. The predominant direction of the electron flow is along the normal to the cathode surface, i.e. along the plasma flux axis. These run-away electrons produce an ambipolar electric field, which, in turn, accelerates ions from the front of the plasma jet up to the high energies. This conclusion is in qualitative agreement with the results of the angular measurements presented above,

which have found that ions with high energies originated at the beginning of the pulse, propagated within a narrow solid angle. Throughout the pulse, the angular distributions of both the ion flux density and average ion energy spread out and approach the commonly measured steady-state distributions. This spreading reduces the ion flux moving along the axis that results in a decrease in ions passing the entrance orifice of the ion energy analyzer, which, in turn, cause the observed abrupt drops with time of ion signal from the analyzer (figure 3(d)–(f)).

At the moment any complete theory describing ion acceleration due to the effect of the self-consistent electrical field originating at the plasma flux of a pulsed vacuum discharge is absent. Just note the recent work of Shmelev and Barengolts [32], where they presented the results of a computer simulation of the process of anomalous ion acceleration in the spark stage of a vacuum discharge. They showed that this acceleration is due to the presence of a plasma cloud in the interelectrode gap, where development of a strong electron instability during the propagation of a cathode electron beam leads to potential buildup to a level exceeding the applied voltage. The values E_{ml}/Z held nearly constant for different ion species and the pronounced tail of the fast ions that is oriented *along the axis* of the plasma flux is present as well. These results are in qualitative agreement with our experimental data.

Finally, note that both effects, namely decay throughout a pulsed arc of the ion energies studied in the present paper as well as the similar decay of the ion charge state observed earlier by other researchers may also be explained by collisions with neutrals. The neutrals are present in cathode arc plasmas because of evaporating macroparticles, hot craters and desorption of the residue gas from walls of the vacuum vessel [33, 34].

4. Conclusion

For all investigated cathode materials with different electro- and thermo-physical characteristics, a significant increase in both the directed energy and the width of 'momentary' IEDs measured at the initial stage of the pulsed arc as compared with those measured at the subsequent steady-state stage were observed. A few mechanisms are suggested as being responsible for the effect observed. The inherent features of the accelerated ions are as follows: (i) the directed energies per charge unit are close to each other for cathode materials with different average ion charge states; (ii) rather extended 'tails' of ions accelerated up to a few hundred electronvolts are present at IEDs, which results in a strong non-Maxwellian shape of the IED and (iii) the fact that these ions propagate just within a narrow angle relative to the flux axis suggests that the preferred mechanism of the additional ion acceleration at the initial stage of a pulsed arc is due to a self-consistent electrical field arising in front of the plasma flow. However, additional studies are needed to support the supposition.

Acknowledgments

This work was supported in part by the programme 'Development of Scientific Potential in Higher Schools' (projects 2.1.1/5955 and 2.1.1/4222).

References

[1] Anders A and Yushkov G Yu 2002 *J. Phys. D: Appl. Phys.* **91** 4824
[2] Bugaev A S, Gushenets V I, Nikolaev A G, Oks E M and Yushkov G Yu 1999 *IEEE Trans. Plasma Sci.* **27** 882
[3] Bugaev A S, Gushenets V I, Nikolaev A G, Oks E M and Yushkov G Yu 2000 *Tech. Phys.* **45** 1135
[4] Yushkov G Y, Anders A, Oks E M and Brown I G 2000 *J. Appl. Phys.* **88** 5618
[5] Bugaev A S, Oks E M, Yushkov G Y, Anders A and Brown I G 2000 *Rev. Sci. Instrum.* **71** 701
[6] Yushkov G 2000 *Proc. 20th ISDEIV (Xi'an, China)* p 260
[7] Anders A and Oks E M 2007 *J. Appl. Phys.* **102** 043304
[8] Galonska M, Hollinger R and Spädtke P 2004 *Rev. Sci. Instrum.* **75** 1592
[9] Chhowalla M 2003 *Appl. Phys. Lett.* **83** 1542
[10] Kutzner J and Miller H C 1992 *J. Phys. D: Appl. Phys.* **25** 686
[11] Lunev V M, Padalka V G and Khoroshikh V M 1977 *Sov. Phys.—Tech. Phys.* **22** 858
[12] Rosén J, Anders A, Mráz S and Schneider J M 2005 *J. Appl. Phys.* **97** 103306
[13] Anders A, Anders S, Jüttner B and Brown I G 1993 *IEEE Trans. Plasma Sci.* **21** 305
[14] Reich H, Spädtke P and Oks E 2000 *Rev. Sci. Instrum.* **71** 707
[15] Anders A 2001 *IEEE Trans.Plasma Sci.* **29** 393
[16] Plyutto A A, Ryzhkov V N and Kapin A T 1965 *Sov. Phys.—JETP* **20** 328
[17] Wieckert C 1987 *Contrib. Plasma Phys.* **27** 309
[18] Beilis I I, Lyubimov G A and Zektzer 1988 *Sov. Phys.—Tech. Phys.* **33** 1132
[19] Chen F F 1965 *Plasma Diagnostic Techniques* ed R H Huddlestone and S L Leonard (New York: Academic)
[20] Anders A, Brown I, MacGill R and Dickinson M 1996 *Rev. Sci. Instrum.* **67** 1202
[21] Siemroth P, Schülke T and Witke T 1995 *IEEE Trans. Plasma Sci.* **23** 919
[22] Beilis I, Djakov B E, Jüttner B and Pursch H 1997 *J. Phys. D: Appl. Phys.* **30** 119
[23] Gidalevich E, Boxman R L and Goldsmith S 1998 *J. Phys. D: Appl. Phys.* **31** 304
[24] Jüttner B 1999 *IEEE Trans. Plasma Sci.* **27** 836
[25] Jüttner B, Djakov B E, Schülke T and Siemroth P 1996 *Proc. 17th ISDEIV (Berkeley, CA)* p 123
[26] Krinberg I A and Zverev E A 2003 *Plasma Sources Sci. Technol.* **12** 372
[27] Krinberg I A 2001 *Tech. Phys. Lett.* **27** 45
[28] Kimblin C W 1973 *J. Appl. Phys.* **44** 3074
[29] Beilis I 2005 *IEEE Trans. Plasma Sci.* **33** 1537
[30] Mesyats G A 2000 *Cathode Phenomena in a Vacuum Discharge: The Breakdown, the Spark and the Arc* (Moscow: Nauka)
[31] Muzukin I L 2005 *IEEE Trans. Plasma Sci.* B **33** 1560
[32] Shmelev D and Barengolts S 2008 *Proc. 23rd ISDEIV (Bucharest, Romania)* p 519
[33] Anders A 2005 *IEEE Trans. Plasma Sci.* **33** 205
[34] Yushkov G Yu and Anders A 2007 *IEEE Trans. Plasma Sci.* **35** 516